International Journal of Modern Physics B
Vol. 28, No. 7 (2014) 1450016 (9 pages)

DOI: 10.1142/S0217979214500167

FROZEN MODE IN PHOTONIC CRYSTAL WAVEGUIDE

YE LIU*,†, LIN LUO† and CHUN JIANG†,‡

*College of Fundamental Studies, Shanghai University of Engineering Science, Shanghai 201620, P. R. China

†State Key Laboratory of Advanced Optical Communication Systems and Networks, Shanghai Jiao Tong University, Shanghai 200240, P. R. China

*yeliu@sues.edu.cn

‡cjiang@sjtu.edu.cn

Received 22 May 2013
Revised 13 October 2013
Accepted 18 October 2013
Published 27 November 2013

We propose a structure of 2D photonic crystal waveguide composed of hexagonal lattices of air holes in high index materials. Frozen mode regime can be observed within the photonic band gap. Light incident into the waveguide is coupled into two modes. One mode has enhanced amplitude and the other one has slow group velocity. Finite-different time-domain (FDTD) simulation is used to demonstrate the propagation of the slow mode.

Keywords: Photonic crystal waveguides; slow light.

PACS numbers: 42.15.-i, 42.79.Gn, 42.82.Et

1. Introduction

Slow light has recently sparked research interest due to its potential application in telecommunication and optical data processing, such as all-optical buffers and optical storages. Light-matter interaction can be enhanced due to the spatial compression of the optical pulses.[1] The approaches pursued to obtain slow light can be categorized into two major mechanisms. One is based on the material dispersion, such as the effect of electromagnetically induced transparency (EIT).[2,3] The other one is using the structural dispersion[4–20] without involving any intrinsic resonant excitations. Based on the latter, slow light in photonic crystal waveguides (PhCW), has been extensively investigated due to its unique physical characteristics.

The unique situation, referred to as frozen mode in slow light region, has been proposed in magnetic photonic crystals.[21] Such modes occur at the stationary inflection points of the dispersion relations, whose first-order and second-order derivatives of angular frequency with respect to wavevector are zero, whereas the third-order

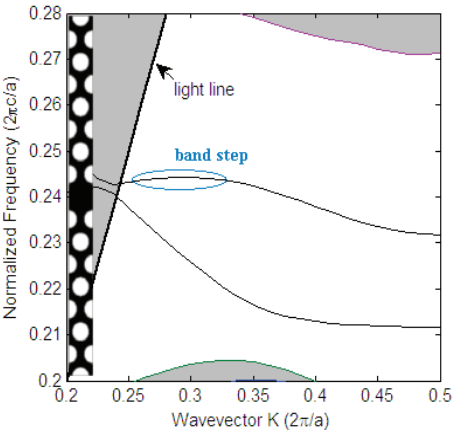

Fig. 1. Dispersion diagram of a typical conventional W1 PhCW with hexagonal lattice of air in Si background, where the radius $r = 0.30\,a$. The left inset sketches a unit supercell of the PhCW in our calculation. The thick line represents the air light line.

derivative is nonzero. Light with proper frequency and polarization can be completely converted into the slow frozen mode with a zero group velocity and drastically enhanced amplitude. Such modes have shown huge potentials for its practical applications. Later, the same research team suggested that oblique frozen mode can also be realized in these specially designed anisotropic layers of nonmagnetic photonic crystals.[22–24] It was reported that the inflection point could be obtained in the PhCW with three rows of air hole located at central line-defect waveguides,[25] while Ref. 26 has presented the experiment realization of such PhCW, showing the light behavior at the unique flat band. Reference 27 also presented an inflection point in the PhCW with a row of elliptical air hole added into the central line-defect waveguides. In this paper, we propose a simple two-dimensional (2D) photonic crystal line-defect waveguide with a stationary inflection point contained in its dispersion relation, where frozen mode can be observed.

As shown in the typical band diagram of conventional W1 PhCW, Fig. 1 illustrates a semi-step band of odd mode lying in the frequency region ranging from 0.22 to 0.35 $(2\pi/a)$, where a is the lattice constant. Changing the values of parameters of the conventional PhCW, such as radius of the holes or the width of the waveguide, may result in the unique frozen mode with an inflection point in our 2D structure. The thick line is the air light line and the gray regions show the light core above the light line and the slab mode regions.

The structure of the paper is arranged as follows. First, an ideal band is presented with a stationary inflection point, resulting in the frozen mode regime. The process of parameters detuning is shown. The band structure is calculated by plane wave expansion method (PWE).[28] Next, the corresponding frozen mode and the unique light propagation are demonstrated by finite-difference time-domain method (FDTD).[29]

2. Design of Dislocated PhCW

In PhCWs, the speed of light is always defined as the optical group velocity v_g, which describes the speed at which a pulse envelope propagates,

$$v_g = \frac{d\omega}{dk}\,, \tag{1}$$

where k is the Bloch wave vector and $\omega = \omega(k)$ is the corresponding frequency. At the stationary inflection point $\omega = \omega_0$, where the dispersion relation of the PhCW is given as

$$\frac{d\omega}{dk} = 0\,, \quad \frac{d^2\omega}{dk^2} = 0\,, \quad \frac{d^3\omega}{dk^3} \neq 0\,. \tag{2}$$

The frequency ω_0 of inflection point is a so-called frozen mode point.[30] The whole process of searching for such a stationary inflection point with frozen mode is shown in the contents below.

The structure of the PhCW we investigated is illustrated in Fig. 2. The proposed structure is based on a 2D silicon ($n = 3.5$) PhC consisting of hexagonal lattices of air holes in Si. The lattice constant is denoted as a and the basic airhole diameter is $2R$. Here the magnetic field perpendicular to the periodic plane is considered only, namely the TE mode because that the TM band gap in triangle lattice PhC is too narrow. The diameters of the basic air holes ($2R$) and air holes adjacent to the line-defect waveguide ($2r$) are chosen to be variable parameters. Especially, the relative position of the two claddings at the two sides of the line-defect waveguide can be shifted. We assume that the parameters of one of the two claddings and line-defect waveguide are fixed. The value of the shifting of other cladding is denoted as v. All the parameters are pointed out in Fig. 2.

First, in order to get a flat step-band, the radius of air holes R is changed from $0.26\,a$ to $0.36\,a$, as shown in Fig. 3(a). One can see that the step-band become flatter as R increases, and then the trend becomes blurred. Considering that modes

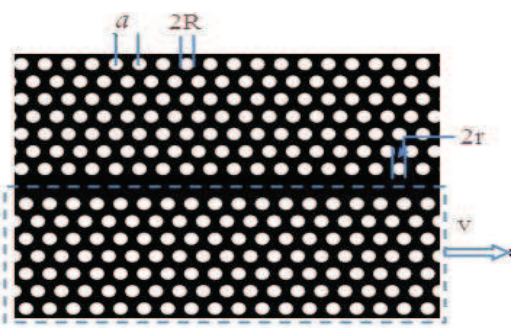

Fig. 2. Schematic of the waveguide structure with hexagonal lattice of air hole radius $R = 0.3\,a$, the index of background is $n = 3.5$. All the parameters marked in the figure are shifted in order to get the inflection points. v means to move the holes in the bottom cladding (marked by the dashed rectangle) by v along the x-axis, compared to the cladding in the top of the waveguide.

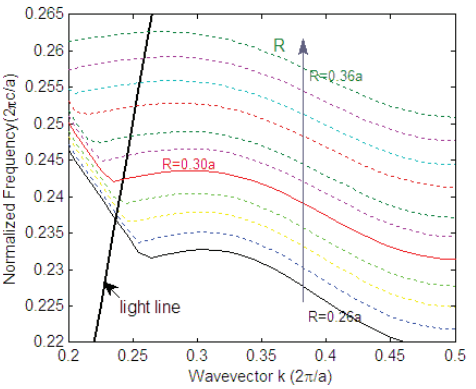

(a)

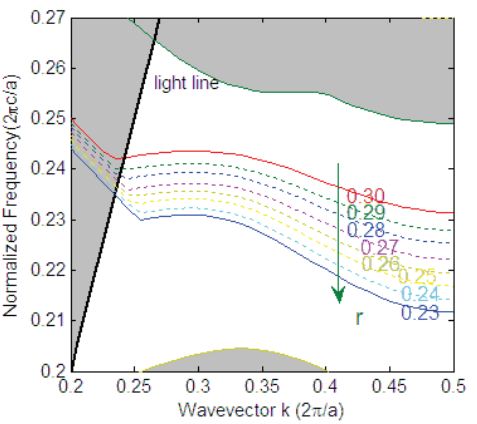

(b)

Fig. 3. (a) The shifting tendency of the flat-step-band changes when the radius of air holes R is shifted ($R = 0.26\,a - 0.36\,a$). (b) The shifting tendency of band changes when the radius r of air holes is just next to the waveguide, where R is set to be $0.3\,a$.

above the light line would couple into radiation modes and would be leaky, the modes with entire step-band regime lying below the light line are preferred. Thus, the $R = 0.30\,a$ is chosen for further study. The first band gap of the TE mode of the photonic crystal with $R = 0.30\,a$ ranges from 0.2050 to 0.2724 $(2\pi/a)$, calculated by the PWE method. Actually, there are two modes lying in the band gap, as are shown in Fig. 1. However, focus is directed to search for a stationary inflection point, and what really interests us here is the step-band of the even mode.

Then, we move on to study the dependence of the step-band on the radius of the air holes adjacent to the line-defect waveguide. The diameter of the basic air holes is fixed to be $0.3 \times 2 = 0.6\,a$. The diameter dependence of the band is shown in Fig. 3(b). For $r = 0.24 - 0.30\,a$, the band in the target step-band regime becomes flatter as r increases.

Next, without changing r, we check out how the dislocation influences the band. Still, the diameters of both basic air holes R and r are set to be $0.3\,a$. The dislocation is formed by dragging the holes of one cladding along x-axis by v, as is illustrated in Fig. 2. Figure 4(a) demonstrates how the dislocation between the two claddings up and below the waveguide changes the tendency of the flat-band. There are two stationary points in each band modes, marked by the ellipses, A and A′, B and B′, respectively. The second derivatives at A and A′ are opposite, thus it can be inferred that points with zero second derivative could be sandwiched between the pairs of stationary points. What we have to do next is to figure out whether a band with stationary inflection point exists or not. For $v = 0 - 0.3$, as v increases, the band become flatter and flatter and then off-level. The critical value of the dislocation

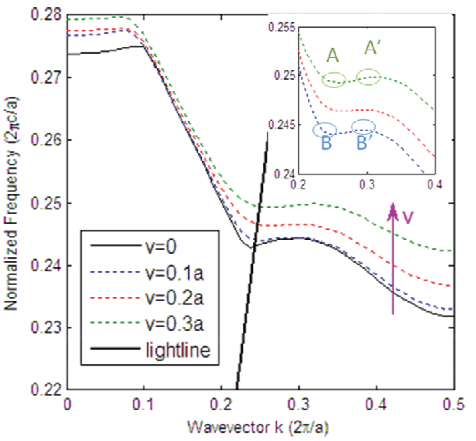

(a)

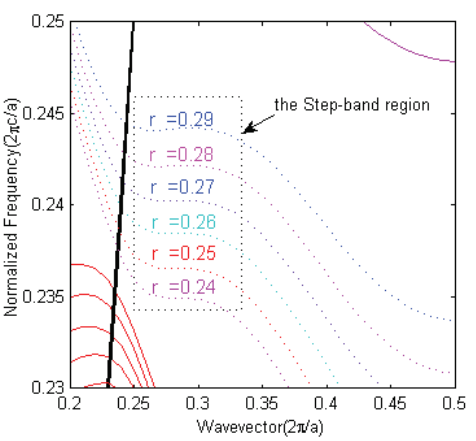

(b)

Fig. 4. (a) The dependence of the step-band on dislocation v. A flatten step-band is shown as the red curve, namely $v = 0.2\,a$. (b) The dependence of step-band on r, where v is fit to be $0.2\,a$.

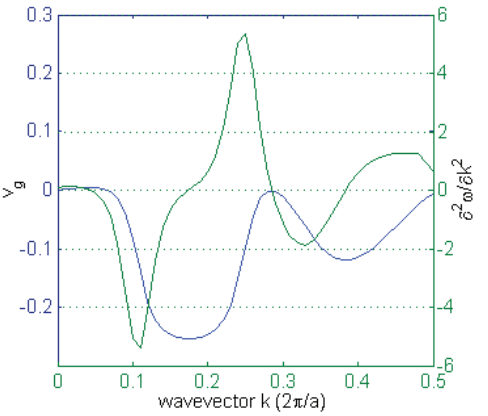

Fig. 5. The group velocity and the second-order derivatives of frequency.

v is equal to $0.2\,a$, indicating that the cladding below is shifted by $0.2\,a$ along the x-axis. The right inset sketches a window with the enlarged flat-band, from which the step-band can be seen more clearly.

Now both of the two parameters are taken into consideration. Setting $v = 0.2\,a$, we let r shift smoothly. The band diagrams are shown in Fig. 4(b). It illustrates that the band would become flatter as r decreases. Finally, it can be seen from the figure that a single inflection point has been obtained at $r = 0.24$ as anticipated. The first- and second-order derivatives are shown in Fig. 5. It clearly illustrates that the first- and second-order derivatives are almost equal to zero at $k = 0.28$, where the respective frequency is 0.2349 $(2\pi c/a)$.

3. FDTD Demonstration

In this section, a FDTD simulation of the 2D PhCW with optimal flat step band is shown. Perfectly matched absorbing boundary layers (PML) are applied to the boundary of the whole structure.[16] The radius of air holes is set to be $R = 0.3\,a$, the dislocation $v = 0.2\,a$ and the radius of the row of air holes in the vicinity of the waveguide to be $r = 0.24\,a$. All these optimized values of the parameters are derived in the calculations above.

To demonstrate the propagation of the unique mode, we assume the wavelength $\lambda \sim 1.55$ μm and thus $a = \nu \times \lambda = 0.2349 \times 1.55 = 0.364$ μm. The structure of the waveguide is shown in Fig. 6(a). The total length $L = 300\,a$. PML are applied to the surrounding of the structure. The frequency center of the Gaussian pulses is $\omega = 0.2349$ $(2\pi c/a)$ and the frequency width is $\Delta\omega = 0.001$ $(2\pi c/a)$. The light source is set at the very beginning of the waveguide. Serials of detectors are put at different positions in the waveguide. The flux result is shown in Fig. 6(b). The fluxes at the 2nd–7th monitors are enlarged to be almost five times as the first monitor. Moreover, it can be seen that the flux is divided into two branches, a larger flux

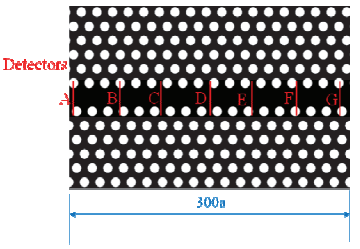

(a)

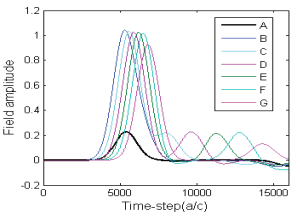

(b)

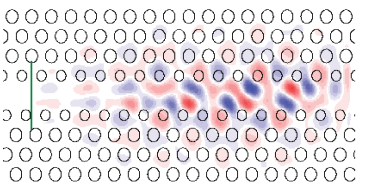

Snapshot of H field at t time steps

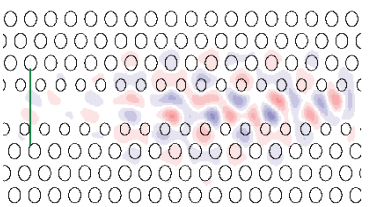

Snapshot of H field at t+400 time steps

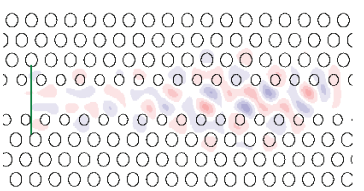

Snapshot of H field at t+600 time steps

(c)

Fig. 6. (Color online) (a) Schematic of FDTD simulation of our proposed step-band waveguides. Red lines in the waveguide mark these detectors to collect the signal of flux. (b) Field amplitude of the proposed PhCW recorded at different positions of the waveguide. Light source with the center frequency 0.2349 ($2\pi c/a$) is set at the front part of the waveguide. The thick blue curve is the amplitude detected at the input, while the thin blue one is at the output. (c) The snapshots of H field pattern of the frozen mode recorded at different time-step.

and a smaller one, indicating that the input light is coupled to the two modes; one mode corresponds to the large flux and the other mode, the smaller flux. The mode with larger flux propagates through the waveguide in such a quick time since it only spends less than 2000 time steps.

The mode with smaller flux, whose amplitude is much similar to the input, propagates through the waveguide with slow light properties and nondistortion. As seen from the figure, the time step interval between input and output fluxes, in other words, the thick blue and thin blue curves, is nearly 1.0×10^4, thus the group velocity is estimated to be 3×10^{-2} c.

The snapshots of mode pattern of the frozen mode recorded at different time-steps are shown in Fig. 6(c). The waveguide is a sectional drawing of the very beginning of our waveguides. We can see from the three snapshots that the slow mode is still localized in the very front part of the waveguide that it has not been monitored by the monitors placed in Fig. 6(a), the slow mode decays due to leakage loss caused by limited rows of the transverse air holes. It can be inferred that this is the frozen mode that is sought.

4. Conclusion

In this paper, we have proposed a structure of 2D PhCW which is composed of a unique TE mode band structure. By adjusting the parameters carefully, such as the diameters of air holes and the dislocation of the two claddings, the phenomenon of frozen mode occurs. Light incident into the waveguide can couple into two modes: one with a small group velocity and the other with drastically enhanced amplitude.

Acknowledgments

This work was supported by the National Natural Science Foundation of China (Grant Nos. 61177056 and 61205052) and sponsored by Shanghai Pujiang Program.

References

1. E. Yablonovitch, *Phys. Rev. Lett.* **58**, 2059 (1987).
2. S. John, *Phys. Rev. Lett.* **58**, 2486 (1987).
3. T. F. Krauss, *J. Phys. D: Appl. Phys.* **40**, 2666 (2007).
4. T. Baba, *Nat. Photon.* **2**, 465 (2008).
5. L. H. Frandsen *et al.*, *Opt. Expr.* **14**, 9444 (2006).
6. A. Yu. Petrove and M. Eich, *Appl. Phys. Lett.* **85**, 4866 (2004).
7. T. Baba *et al.*, *Opt. Expr.* **16**, 9245 (2008).
8. S.-C. Huang *et al.*, *Opt. Expr.* **15**, 3543 (2007).
9. J. Ma and C. Jiang, *IEEE. Photon. Technol. Lett.* **20**(14), 1237 (2008).
10. J. He *et al.*, *Opt. Expr.* **16**, 11077 (2008).
11. J. Hugonin *et al.*, *Opt. Lett.* **32**, 2638 (2007).
12. S. Ha *et al.*, *Opt. Expr.* **16**, 1104 (2008).
13. D. Mori *et al.*, *Opt. Expr.* **15**, 5264 (2007).
14. M. Settle *et al.*, *Opt. Expr.* **15**, 219 (2007).

15. J. Brosi, J. Leuthold and W. Freude, *J. Lightwave Technol.* **25**, 2502 (2007).
16. S. Mingaleev, A. Miroshnichenko and Y. Kivshar, *Opt. Expr.* **15**, 12380 (2007).
17. D. Beggs *et al.*, *Opt. Lett.* **33**, 147 (2008).
18. L. Frandsen *et al.*, *Opt. Expr.* **14**, 9444 (2006).
19. Säynätjoki *et al.*, *Opt. Expr.* **15**, 8323 (2007).
20. H.-B. Zhang, J.-J. Chen and X. Han, *Int. J. Mod. Phys. B* **26**, 1250133 (2012).
21. A. Figotin and I. Vitebskiy, *Phys. Rev. B* **67**, 165210 (2003).
22. A. Figotin and I. Vitebskiy, *Phys. Rev. E* **68**, 036609 (2003).
23. J. Ballato *et al.*, *Phys. Rev. E* **71**, 036612 (2005).
24. A. Figotin and I. Vitebskiy, *Phys. Rev. E* **74**, 066613 (2005).
25. D. Mori and T. Baba, *Opt. Expr.* **13**, 9398 (2005).
26. S.-C. Huang *et al.*, *Opt. Expr.* **15**, 3543 (2007).
27. F. Wang, J. Ma and C. Jiang, *J. Lightwave Technol.* **26**, 1381 (2008).
28. S. G. Johnson and J. D. Joannopoulos, *Opt. Expr.* **8**, 173 (2001).
29. A. Taflove, *Computational Electrodynamics, the Finite Difference Time Domain* (Artech House, Boston, MA, 1995).
30. A. Figotin and I. Vitebskiy, *Waves Random Complex Media* **16**, 293 (2006).